Journal Name

COMMUNICATION

Spatially controlled clustering of nucleotide-stabilized vesicles †

Subhabrata Maiti,[a,b] Ilaria Fortunati,[a] Ayusman Sen,[b] and Leonard J. Prins *[a]

Received 00th January 20xx,
Accepted 00th January 20xx

DOI: 10.1039/x0xx00000x

www.rsc.org/

The hierarchical self-assembly of surfactant molecules into large clusters of vesicles is described. The two-step process relies on the initial stabilization of vesicles by guanosine monophosphate followed by Ag^+-induced aggregation of the vesicles in micrometer-sized colonies. Spatial control over aggregation is obtained by locally generating Ag^+-ions through oxidation of a Ag-surface.

The hierarchical organization of molecules into large multicellular structures is one of the fascinating features of living organisms.[1,2] An important aspect of organisms is their colonization in an environment which allows growth.[3] For instance, studies related to origin-of-life have shown that unicellular algae become multicellular owing to the presence of different iron containing surfaces, like FeS or other mineral clays, by utilizing specific metal-ion uptake mechanisms (for example, iron).[4-7] This fact inspired us to develop a synthetic system that mimics the biological hierarchical self-assembly of small molecules into multicellular structures. This would provide a model system for studying biological processes and properties associated to higher-order structures, such as communication, cooperativity, transport and catalysis.[8-13] The first step involves the nucleotide-triggered self-assembly of individual surfactant molecules into vesicles which, in a second step, cluster into larger aggregates. This latter step is triggered by metal ions, which are released from a metal surface. This is an important feature, because it provides a straightforward tool to induce concentration gradients in a solution, which is currently attracting a strong interest in out-of-equilibrium chemistry, and permits programmable surface patterning.[14-18]

We recently showed that adenosine triphosphate (ATP) can stabilize vesicular aggregates composed of surfactant C_{16}TACN·Zn^{2+} in aqueous buffered solution (TACN = 1,4,7-triazacyclononane).[19-20] The presence of ATP caused a 10-fold decrease in the critical aggregation concentration of C_{16}TACN·Zn^{2+} (*cac*) from around 100 µM to 10 µM, which implies that ATP can induce aggregation at concentrations at which the surfactant molecules by themselves are not in an aggregated state. This effect is ascribed to (partial) charge neutralization on the surface and the interaction of a single ATP molecule with multiple surfactant molecules leading to a preorganization of the latter. We hypothesized that this first self-assembly step could form the basis for the formation of higher order structures by introducing additional recognition elements in the system. Our strategy relied on the use of guanosine monophosphate (GMP) rather than ATP as templating agent for vesicle formation,[21] because it is known that the formation of coordination bonds between an Ag^+-ion and the N7 of the guanine nucleobase causes self-assembly of multiple GMP units.[22] Previously we have shown that this interaction can be exploited to develop a Ag^+-sensing system based on Au NPs functionalized with the same TACN·Zn^{2+} complex.[23,24] In the present system, we expected that the addition of Ag^+-ions to GMP-stabilized vesicles would lead to vesicle clustering (Fig. 1).

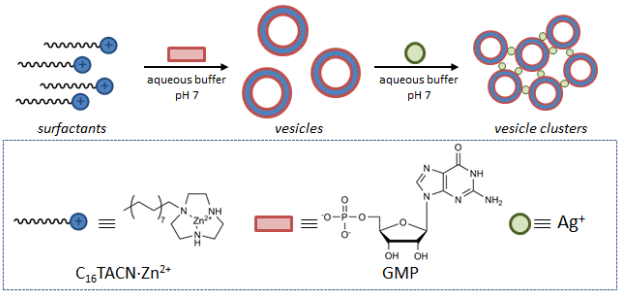

Fig. 1 Schematic representation of GMP-templated formation of vesicular aggregates and their successive clustering in larger aggregates by $AgNO_3$.

The ability of GMP to induce aggregate formation was confirmed by a titration experiment in which the concentration of C_{16}TACN·Zn^{2+} was gradually increased in the presence of a constant concentration of GMP (20 µM) and the fluorescent apolar probe 1,6-diphenyl-1,3,5-hexatriene (DPH, 2.5 µM, λ_{ex} = 355 nm, λ_{em} = 428 nm). DPH is solubilized by the apolar part of surfactant-based aggregates and consequently a

[a] Department of Chemical Sciences, University of Padova, Via Marzolo 1, 35131 Padova, Italy, Email: leonard.prins@unipd.it.
[b] Department of Chemistry, The Pennsylvania State University, University Park, PA-16801, USA

† Electronic Supplementary Information (ESI) available: Experimental methods, spectroscopic data, TEM, confocal and optical microscopic images, supporting videos. See DOI: 10.1039/x0xx00000x

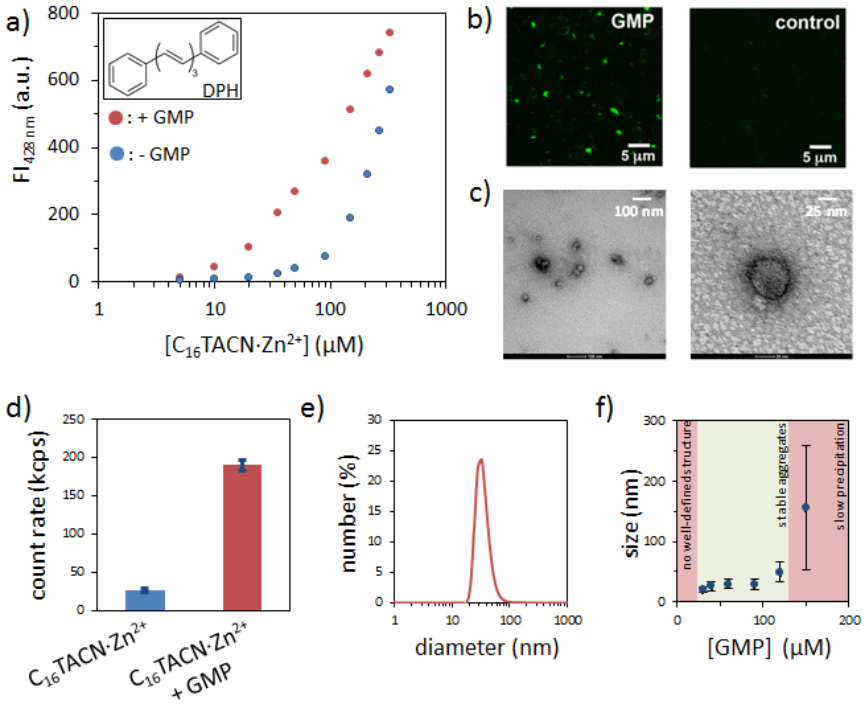

Fig. 2 Characterization of GMP-stabilized vesicles. a) Fluorescence intensity at 428 nm as a function of the amount of the $C_{16}TACN{\cdot}Zn^{2+}$ added to an aqueous buffer solution in the presence or absence of a fixed concentration of GMP (20 μM); excitation wavelength = 355 nm, slit width (ex/em) = 5/10 nm. b) Confocal images of a surfactant solution without and with GMP (20 minutes after mixing). Samples contained $C_{16}TACN{\cdot}Zn^{2+}$ (30 μM), C153 (2.5 μM) and GMP (45 μM). Experimental conditions: [HEPES] = 5 mM, pH 7.0, T = 22 °C. c) TEM images of a solution containing GMP (45 μM) and $C_{16}TACN{\cdot}Zn^{2+}$ (30 μM) in HEPES buffer (pH = 7, 5 mM). Samples were stained with 2 % uranyl acetate solution. (d) Scattering intensity rate (count rate, kcps) measured by dynamic light scattering (DLS) of the aggregates formed in the absence and presence of GMP (45 μM) and a fixed amount of $C_{16}TACN{\cdot}Zn^{2+}$ (30 μM). (e) Representative DLS profile of aggregates in a solution containing GMP (40 μM) and $C_{16}TACN{\cdot}Zn^{2+}$ (30 μM). Experimental conditions: [HEPES] = 5 mM, pH 7, T = 25 °C. (f) Hydrodynamic diameter values measured by DLS as a function of GMP concentration (10 – 150 μM) at a constant concentration of $C_{16}TACN{\cdot}Zn^{2+}$ (30 μM) in HEPES buffer (pH = 7, 5 mM). The green area indicates the concentration regime at which stable aggregates were observed.

significant increase in fluorescence intensity is observed when aggregates are formed. It was observed that the fluorescence intensity started to increase significantly after the addition of 20 μM of surfactant, compared to a concentration of around 100 μM in the absence of GMP (Fig. 2a). The propensity of GMP to stabilize aggregates of $C_{16}TACN{\cdot}Zn^{2+}$ emerged also from an inverse titration in which increasing amounts of GMP were added to a 30 μM solution of the surfactant, which is well below the *cac* of 100 μM. Addition of GMP caused a rapid increase in fluorescence intensity at low micromolar concentrations (0 - 10 μM) and a saturation level was reached at around 50 μM (Fig. S1, Electronic supplementary information (ESI)). Additional confirmation of aggregate formation was obtained from other techniques: UV-Vis, confocal laser scanning microscopy, DLS and TEM. UV-vis spectra of GMP were measured in the 5 - 60 μM concentration regime in the presence and absence of $C_{16}TACN{\cdot}Zn^{2+}$ (30 μM; Fig. S2+S3, ESI). The difference in absorbance between the two data sets showed a clear dependence on the concentration of GMP, indicative of a direct interaction between GMP and the $TACN{\cdot}Zn^{2+}$ head group (Fig. S3). Confocal laser scanning microscopy studies permitted a direct visualization of aggregate formation. Although the size of the aggregates (*vide infra*) is lower than the resolution of this optical technique, the aggregation of the hydrophobic probe coumarin153 (C153) in the aggregates resulted in an increase in local probe concentration which could be detected. Aggregates were detected upon the addition of GMP (45 μM) to a solution of $C_{16}TACN{\cdot}Zn^{2+}$ (30 μM) and C153 (2.5 μM) (Fig. 2b,c). Control experiments with a regular fluorescence spectrophotometer confirmed that the C153 fluorescence increased significantly only in the presence of GMP, just as observed for the DPH-probe (Fig. S4). The dynamic light scattering (DLS) intensity (count rate, kcps) of a 30 μM $C_{16}TACN{\cdot}Zn^{2+}$-solution increased significantly when GMP (45 μM) was added (Fig. 2d). Altogether, these data show that the GMP plays an important role in stabilizing $C_{16}TACN{\cdot}Zn^{2+}$-based aggregates. We assume that this originates from direct interactions between guanine and the $TACN{\cdot}Zn^{2+}$-complex supported by the UV-Vis titrations - in addition to the electrostatic interactions originating from the phosphate-group.[21,25]

Next, we analyzed the structure of the GMP-templated aggregate by DLS and TEM. We performed a series of DLS measurements of solutions containing a constant concentration of surfactant (30 μM) and varying concentrations of GMP (10 - 150 μM). Stable aggregates with a well-defined size of 31 ± 10 nm were obtained for GMP concentrations between 30 and 120 μM (Fig. 2e,f, Fig. S5). At lower concentrations, no reproducible sizes could be measured, whereas at higher concentrations very large aggregates were observed which tended to precipitate. TEM images revealed the formation of spherical aggregates with similar dimensions (Fig. 2c, Fig. S6). Considering that the fluorescent probes revealed the presence of a hydrophobic domain in these aggregates and also based on detailed previous studies of a related system, we postulate that GMP templates the formation of vesicle-like aggregates.

Next, we were interested in studying the effect of Ag^+-ions on the GMP-stabilized aggregates. Initially, we studied with UV-Vis spectroscopy the interaction between Ag^+ and GMP in the absence of surfactant. It is noted that a decrease in the UV absorbance maxima of GMP at 253 nm is a signature characteristic of binding of Ag^+ to the nucleobase.[22] Under the experimental conditions, the titration of $AgNO_3$ to GMP (30 μM) revealed no binding up to a concentration of 150 μM, after which the absorption at 253 nm started to decrease (Fig. S7). However, we were pleased to observe that the same titration performed in the presence of $C_{16}TACN{\cdot}Zn^{2+}$ (30 μM)

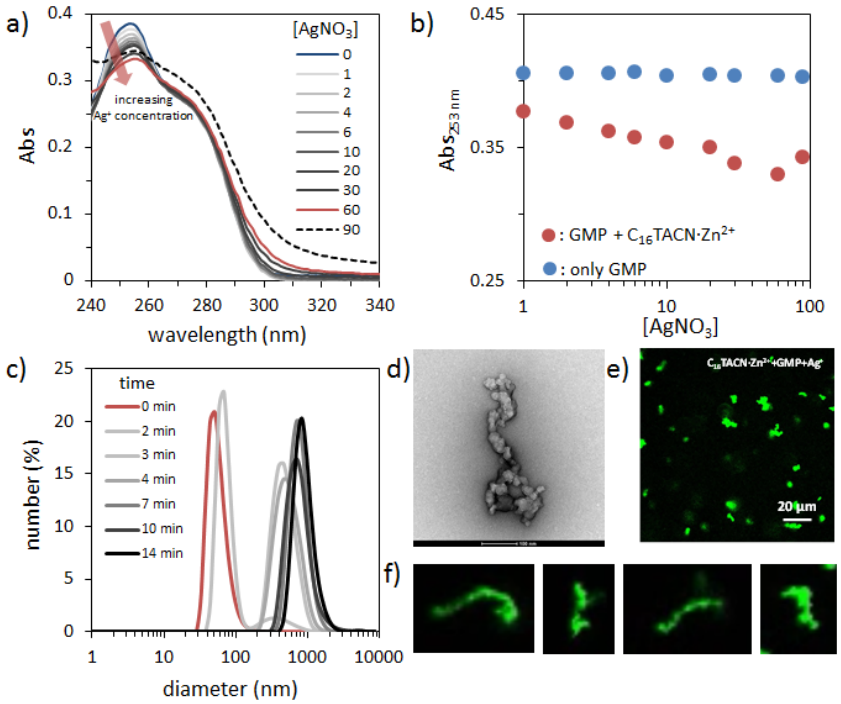

Fig. 3 Characterization of GMP-stabilized vesicles. a) UV-Vis spectra of GMP (30 µM) in the presence of $C_{16}TACN{\cdot}Zn^{2+}$ (30 µM) as a function of the Ag^+-concentration in aqueous HEPES buffer (5 mM, pH 7.0). b) Plot of the absorbance at 253 nm as a function of Ag^+-concentration in the presence and absence of surfactant (see also ESI for details) under the same experimental condition. c) Change in hydrodynamic diameter of the aggregates in time in a solution of $C_{16}TACN{\cdot}Zn^{2+}$ (30 µM), GMP (45 µM) and Ag^+ (30 µM) measured by dynamic light scattering (DLS) in aqueous buffer solution (HEPES, 5 mM, pH 7.0), d) TEM images of the aggregated vesicles with [$C_{16}TACN{\cdot}Zn^{2+}$] = 25 µM, [GMP] = 25 µM and [Ag^+] = 20 µM (stained with 2 % uranyl acetate solution) (scale bar = 100 nm), e) Confocal images taken 30 min after addition of Ag^+ to a sample containing $C_{16}TACN{\cdot}Zn^{2+}$ (100 µM), GMP (100 µM), C153 (2.5 µM). f) Snapshots of single structures taken from supplementary movie S1.

showed a decrease in absorbance already upon the addition of low micromolar concentrations of Ag^+ (Fig. 3a,b). This is interesting because it indicates that the surfactant facilitates complex formation between GMP and Ag^+. It is noted that turbidity was observed at Ag^+-concentrations higher than 100 µM indicating the rapid formation of higher order aggregates. For that reason, we performed an analysis of the formed structures and the kinetics of their formation by DLS, TEM and confocal laser scanning microscopy. Within minutes after addition of $AgNO_3$ solution (30 µM) to GMP-stabilized aggregates ($C_{16}TACN{\cdot}Zn^{2+}$ = 30 µM, GMP = 45 µM) DLS measurements showed a significant increase in size reaching dimensions in the micrometer range (Fig. 3c). TEM images revealed irregular shaped clusters of the same dimensions in which, however, the spherical shapes of the original vesicles could be clearly distinguished (Fig. 3d and Fig. S8). Final compelling evidence for the Ag^+-induced clustering of GMP-stabilized vesicles and a direct insight in the kinetics was obtained from confocal microscopy using the previously described C153 probe. (Fig. 3e-f, Supporting video S1, Fig. S9) After addition of a $AgNO_3$-solution (300 µM) to a solution of GMP-stabilized vesicles ($C_{16}TACN{\cdot}Zn^{2+}$ = 100 µM, GMP = 100 µM) no apparent changes seem to occur for a period of around 12 minutes and only objects corresponding to the vesicles are detected. Then a strong increase in the number of objects occurs over a relatively small period of time. As time proceeds these start to aggregate into large structures with micrometer-sized dimensions. This provides a fascinating real time observation of a supramolecular aggregation process of individual units into large clusters.[26] Importantly such structures were not observed in the absence of either GMP or $C_{16}TACN{\cdot}Zn^{2+}$ (Fig. S10) In addition, structures of this size were neither observed when either one of the monophosphate nucleosides (AMP, TMP and CMP) was used instead of GMP (Fig. S11). Only for CMP smaller aggregates were detected, but these lacked the size and complexity of those observed for GMP. This can be explained by the fact that Ag^+-forms ternary complexes with CMP which may stabilize vesicles.[27] Altogether, these results clearly demonstrate that Ag^+-ions act as a glue that causes the agglomeration of vesicles into large clusters relying on selective interactions between Ag^+ and GMP.

Until now the gain over spatial organizational control by external stimuli is mostly limited to metallic nano/microstructures, whereas reports with soft materials are scarce.[28-29] Thus, extending this possibility to soft structures by chemical pathways adds a new dimension to this field. An attractive feature of metal ions is that they can be easily generated in situ through the chemical oxidation of a metal film. This provides an attractive tool to gain spatiotemporal control over self-assembly processes that rely on the availability of metal ions. Herein, we were curious to see whether this approach could be used to locally induce aggregation of GMP-stabilized vesicles. For this purpose, Ag was deposited on a glass slide and enclosed with a hybridization chamber of 20 mm diameter and 0.6 mm height (Fig. 4a, for experimental details see ESI). GMP-stabilized vesicles were injected inside the chamber along with 0.1 mM H_2O_2 in an aqueous solution buffered at pH 7. In the presence of H_2O_2, metallic Ag is oxidized causing the release of Ag^+ ions in solution.[30] Using a microscope we monitored the formation of aggregates and were pleased to observe that aggregation of vesicles occurred indeed only near the Ag surface (at 0.5-1 mm, Fig.4a,c, Fig. S12+S13 and supporting video S2). Aggregate concentration was strongly reduced at around 2 mm and completely absent at around 3 mm (Fig. S12+S13). The presence of Nile Red permitted also imaging by fluorescence, which confirmed that aggregates only formed in close proximity of the Ag-patch. Importantly, no aggregation was observed in the absence of H_2O_2 indicating that the oxidation of Ag is essential to trigger the process. (Fig. S14). Other control experiment under similar experimental condition, in presence of H_2O_2 but in absence of either GMP or surfactant also did not result in the formation of any structure (Fig.

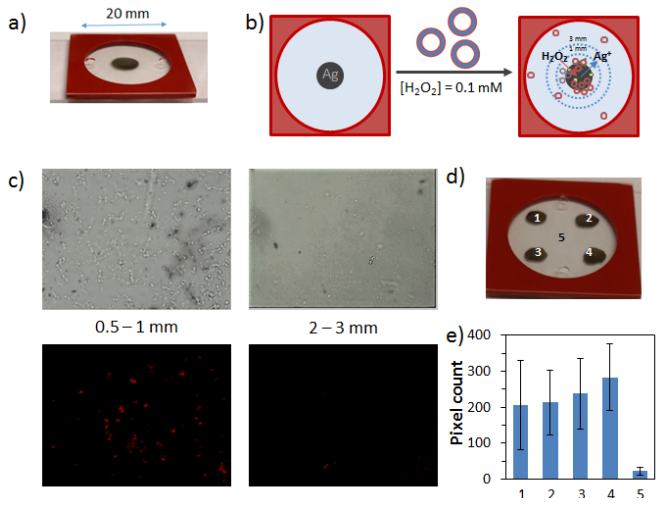

Fig. 4 Spatially controlled induction of vesicle-aggregation. a) Hybridization chamber (*d* = 20 mm) containing a Ag-patch in the center. b) Schematic representation of the local clustering of GMP-stabilized vesicles near the Ag-patch in the presence of H_2O_2. c) Optical and fluorescence microscope images at different distances from the Ag-patch: 0.5-1 mm, and 2-3 mm. Nile red (5 µM) was used as the hydrophobic fluorescence probe. (x-axis of all images = 152.4 µm). Experimental conditions: [C_{16}TACN·Zn^{2+}] = 250 µM, [GMP] = 250 µM, [H_2O_2] = 100 µM, [HEPES] = 5 mM (pH 7.0), T = 25 °C. d) Hybridization chamber (*d* = 20 mm) containing four Ag-patches. e) Statistical analysis (in terms of red pixel count) of the images taken at different positions (numbers refer to Fig. 4d). Four images from two different sets of experiment have been used for the analysis using ImageJ software (parameters: RGB color threshold, Red-75, Green-5, Blue-3).

S15+S16). The observation of similar aggregates in the entire hybridization chamber upon the co-injection of GMP-stabilized vesicles and Ag^+ confirmed that the observed objects indeed result from Ag^+-induced clustering (Figure S17-S20, ESI, supporting video S3). These results encouraged us to create a system in which cluster forming occurs in different areas. Therefore, we have made four Ag-patches as shown in Fig. 4d and added GMP-stabilized vesicle in the presence of H_2O_2 under similar experimental condition. A significantly higher amount of clusters was observed close to the patches (1-4) compared to the central position 5 (Fig. 4e, Fig. S21, ESI).

In conclusion, we have shown the controlled hierarchical self-assembly of small molecules into large structures with micrometer-sized dimensions. The assembly process relies on two consecutive recognition processes, the first one between GMP and the C_{16}TACN·Zn^{2+} leading to nanometer-sized vesicular structures, which, in a second step, cluster into large aggregates driven by the interaction between GMP and Ag^+ metal ions. The controlled activation by means of an oxidation process provides spatial control over the formation of the structures. Overall, the approach provides a facile entry in a class of supramolecular superstructures which are gaining interest because of their applications in the field of sensing and catalysis and, for their function as model systems for studying organization and communication in complex multicellular biological systems.

This work was financially supported by the European Commission (grant MSCA 657486).

Conflicts of interest

There are no conflicts to declare.

Notes and references

1 Z. N. Oltvai and A.–L. Barabási, *Science*, 2002, **298**, 763-764.
2 G. M. Whitesides and B. Grzybowski, *Science* 2002, **295**, 2418-2421.
3 M. Lynch, M. C. Field, H. V. Goodson, H. S. Malik, J. B. Pereira-Leal, D. S. Roos, A. P. Turkewitz and S. Sazeri, *Proc. Natl. Acad. Sci. U.S.A*, 2014, **111**, 16990-16994.
4 G. Wächtershäuser, *Prog. Biophys. Molec. Biol.*, 1992, **58**, 85-201.
5 G. Ertem, *Orig. Life Evol. Biospheres*, 2004, **34**, 549–570.
6 L. J. Prins, *Acc. Chem. Res.*, 2015, **48**, 1920–1928.
7 P. L. Luisi, The Emergence of Life; Cambridge University Press: Cambridge, 2006.
8 W. C. de Vries, D. Grill, M. Tesch, A. Ricker, H. Ngsse, J. Klingauf, A. Studer, V. Gerke and B. J. Ravoo, *Angew. Chem. Int. Ed.*, 2017, **56**, 9603 –9607.
9 O. Roling, C. Wendeln, U. Kauscher, P. Seelheim, H. –J. Galla and B. J. Ravoo, *Langmuir*, 2013, **29**, 10174–10182.
10 X. Wang, R. J. Mart and S. J. Webb, *Org. Biomol. Chem.*, 2007, **5**, 2498-2505.
11 I. C. Pintre and S. J. Webb, *Adv. Phys. Org. Chem.*, 2013, **47**, 129-183.
12 S. Balk, U. Maitra and B. König, *Chem. Commun.*, 2014, **50**, 7852-7854.
13 D. A. Jose and B. König, *Org. Biomol. Chem.*, 2010, **8**, 655-662.
14 E. Mattia and S. Otto, *Nat. Nanotechnol*. 2015, **10**, 111-119.
15 S. O. Krabbenborg, C. Nicosia, P. Chen and J. Huskens, *Nat. Commun.* 2013, **4**, 1667(1-7).
16 M. Sawczyk and R. Klajn, *J. Am. Chem. Soc.*, 2017, **139**, 17973-17978.
17 R. Merindol and A. Walther, *Chem. Soc. Rev.*, 2017, **46**, 5588-5619.
18 S. O. Krabbenborg, J. Veerbeek, J. Huskens, *Chem. Eur. J.*, 2015, **21**, 9638-9644.
19 S. Maiti, I. Fortunati, C. Ferrante, P. Scrimin and L. J. Prins, *Nat. Chem.*, 2016, **8**, 725-731.
20 J. L.-Y. Chen, S. Maiti, I. Fortunati, C. Ferrante and L. J. Prins, *Chem. Eur. J.*, 2017, **23**, 11549 –11559.
21 F. Della Sala, S. Maiti, A. Bonanni, P. Scrimin and L. J. Prins, *Angew. Chem. Int. Ed.*, 2018, **57**, 1611 –1615.
22 K. Loo, N. Degtyareva, J. Park, B. Sengupta, M. Reddish, C. C. Rogers, A. Bryant and J. T. Petty, *J. Phys. Chem. B*, 2010, **114**, 4320–4326.
23 S. Maiti and L. J. Prins, *Chem. Commun.*, 2015, **51**, 5714-5716.
24 S. Maiti and L. J. Prins, *Tetrahedron*, 2017, **73**, 4950-4954.
25 P. Zhou, R. Shi, J. -F Yao, C. –F. Sheng and H. Li, *Coord. Chem. Rev.*, 2015, **292**, 107–143.
26 A. Aliprandi, M. Mauro and L. De Cola, *Nat. Chem.*, 2016, **8**, 10-15.
27 Y. Tanaka, J. Kondo, V. Sychrovsky, J. Sebera, T. Dairaku, H. Saneyoshi, H. Urata, H. Torigoe and A. Ono, *Chem. Commun.*, 2015, **51**, 17343-17360.
28 Y. Kim, A. A. Shah and M. J. Solomon, *Nat. Commun.*, 2014, **5**:3676.
29 A. Altemose, M. A. Sánchez-Farrán, W. Duan, S. Schulz, A. Borhan, V. H. Crespi and A. Sen, *Angew. Chem. Int. Ed.*, 2017, **56**, 7817 –7821.
30 D. He, S. Garg and T. D. Waite, *Langmuir*, 2012, **28**, 10266–10275.